Hindawi
Science and Technology of Nuclear Installations
Volume 2019, Article ID 1673834, 12 pages
https://doi.org/10.1155/2019/1673834

Research Article

Numerical Investigation of Natural Convective Condensation with Noncondensable Gases in the Reactor Containment after Severe Accidents

Wen Fu,[1,2] Li Zhang,[1] Xiaowei Li,[1] and Xinxin Wu[1]

[1]*Key Laboratory of Advanced Reactor Engineering and Safety of Ministry of Education, Collaborative Innovation Center of Advanced Nuclear Energy Technology, Institute of Nuclear and New Energy Technology, Tsinghua University, Beijing 100084, China*
[2]*Luoyang Ship Material Research Institute, Luoyang, Henan 471039, China*

Correspondence should be addressed to Xiaowei Li; lixiaowei@tsinghua.edu.cn

Received 19 July 2018; Accepted 17 January 2019; Published 3 March 2019

Academic Editor: Arkady Serikov

The heat and mass transfer processes of natural convective condensation with noncondensable gases are very important for the passive containment cooling system of water cooled reactors. Numerical simulation of natural convective condensation with noncondensable gases was realized in the Fluent software by adding condensation models. The scaled AP600 containment condensation experiment was simulated to verify the numerical method. It was shown that the developed method can predict natural convective condensation with noncondensable gases well. The velocity, species, and density fields in the scaled AP600 containment were presented. The heat transfer rate distribution and the influences of the mass fraction of air on heat transfer rate were also analyzed. It is found that the driving force of natural convective condensation with noncondensable gases is mainly caused by the mass fraction difference but not temperature difference. The natural convective condensation with noncondensable gases in AP1000 containment was then simulated. The temperature, species, velocity, and heat flux distributions were obtained and analyzed. The upper head of the containment contributes to 35.1% of the total heat transfer rate, while its area only takes 25.4% of the total condensation area of the containment. The influences of the mass fraction of low molecular weight noncondensable gas (hydrogen) on the natural convective condensation were also discussed based on the detailed species, density, and velocity fields. The results show that addition of hydrogen (production of zirconium-water reaction after severe accident) will weaken the intensity of natural convection and the heat and mass transfer processes significantly. When hydrogen contributes to 50% mole fraction of the noncondensable gases, the heat transfer coefficient will be reduced to 45%.

1. Introduction

Safety is the life of nuclear energy. Nuclear power plant takes the concept of defense in depth when designing its safety systems. Reactor containment is the last barrier protecting from leakage of nuclear material. The pressure and temperature in the reactor containment should be kept below the design value to keep its integrity at any accident. The third generation nuclear power plants (such as AP600 and AP1000) introduce passive containment cooling systems to cool their containments and maintain their pressure and temperature below safety limits after severe accident. The heat and mass transfer processes of steam condensation with noncondensable gases after severe accidents are the key phenomena of passive containment cooling system for nuclear power plants [1]. After severe accidents, large amount of air will be present in the containment while steam condensates on the reactor containment wall. Previous investigations showed that a very small amount of noncondensable gases will degrade the heat transfer of condensation significantly [2, 3]. If severe accidents with core melt happen, hydrogen will be generated by Zr-water reaction. This will make the natural convective condensation of steam, air, and hydrogen mixture more complicated [4].

With the condensation of steam, the noncondensable gases tend to accumulate at the interface. The accumulation

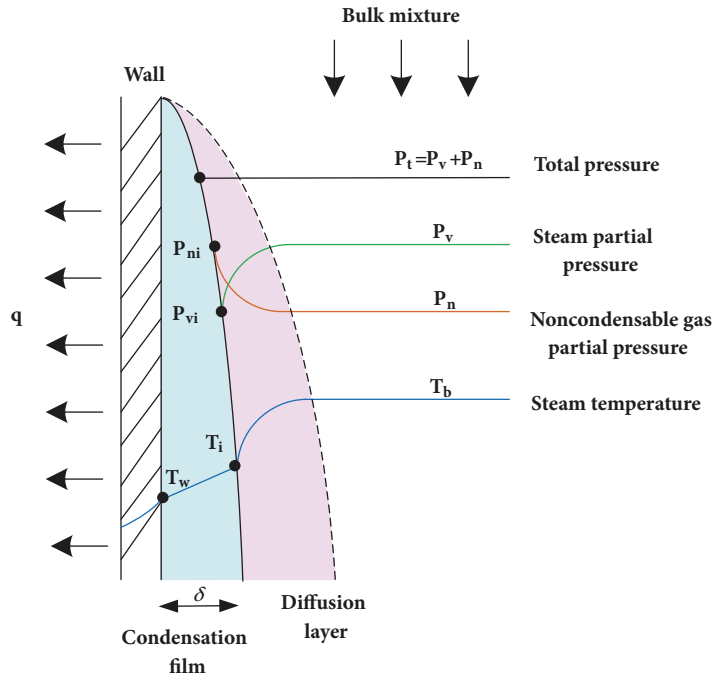

Figure 1: Heat transfer processes of condensation with the presence of noncondensable gases.

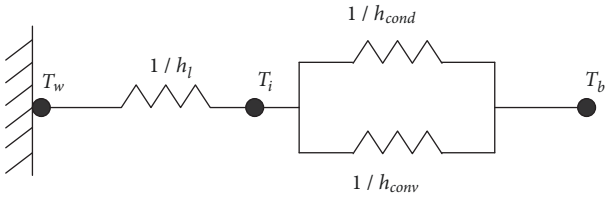

Figure 2: Thermal resistance of condensation with noncondensable gases.

of noncondensable gases at the gas-liquid interface will decrease the heat and mass transfer in two aspects. On one hand, the noncondensable gases inhibit steam diffusing from the gas mixture to the liquid film. On the other hand, since the total pressure remains constant, the accumulation of noncondensable gases also decreases the steam partial pressure and saturation temperature at the interface, which reduces the temperature difference between the interface and the wall, $T_i - T_w$. This is the driving force for steam condensation, as shown in Figure 1. For the heat transfer of condensation with the presence of noncondensable gases, the total heat transfer resistance consists of three parts. As shown in Figure 2., they are the condensation resistance, $1/h_{cond}$, the convection resistance, $1/h_{conv}$, and the conduction resistance of condensation film, $1/h_l$. The total heat transfer resistance can be expressed as

$$R_{total} = \frac{1}{h_l} + \frac{1}{h_g} = \frac{1}{h_l} + \frac{1}{h_{cond} + h_{conv}} \quad (1)$$

A number of experiments have been done to investigate the condensation with noncondensable gases. Empirical correlations were obtained based on the experimental data [5–9]. These correlations can only be used for the verified conditions and geometry. The difference will be large when they are used for different thermal-hydraulic conditions and different geometries. Theoretical research has also been conducted. The heat and mass transfer analogy theory [3, 10–15] was developed. In this method, the pure condensation heat transfer rate (condensation rate) is obtained through the mass and heat analogy. However, the correlations are semiempirical, and some empirical coefficients were needed. In recent years, condensation with the presence of noncondensable gases has been analyzed using computational fluid dynamics method [16–22]. A condensation model is usually not included in commercial CFD software and must be developed by users. Fu et al. [23] realized numerical simulation of the convective condensation of steam-air mixture and steam-helium mixture in vertical tubes through implementing source terms into the conservation equations. The developed numerical method can simulate convective condensation of steam-air mixture well.

The advanced pressurized reactor AP1000 adopts double containments structure, including the inner steel containment and the outer concrete containment. Upon a postulated nuclear plant accident where high pressure and high temperature water escapes into the steel containment in the form of superheated steam, the pressure and temperature in the steel containment will increase. Condensation heat transfer is an important physical process that helps keeping the temperature and pressure in containment within the design limits and ensures the containment integrity. However,

the presence of noncondensable gases in the containment degrades the heat transfer processes. An accurate model for condensation with noncondensable gases is, therefore, essential.

In present work, natural convective condensation with noncondensable gases in the containment will be simulated using the ANSYS FLUENT software. AP600 scaled experiment will be first simulated to verify the numerical method. Then the natural convective condensation in AP1000 containment after severe accident will be simulated. The velocity, species, and density distribution and the effect of hydrogen on steam mixture condensation will be analyzed.

2. Numerical Method

2.1. Geometry and Mesh

2.1.1. Scaled AP600 Containment. The ability of FLUENT software to simulate natural convective condensation with noncondensable gases was examined via simulation of the scaled AP600 containment experiments. Anderson and his coworkers performed the scaled AP600 containment tests at the University of Wisconsin-Madison [8], to investigate the influence of noncondensable gases (air and helium) on steam condensation. The main components of Anderson's experiment facility included the test vessel, the coolant system, and the gas and steam supply system. The rectangular test vessel represented a 1:12 scaled radial slices of the AP600 containment. Anderson carried out atmospheric tests and pressurized tests. This paper only simulates Anderson's "atmospheric tests."

The test vessel has two 0.91 m long aluminum condensing plates, one oriented vertically and the other horizontally. The horizontal condensing plate is in the top right hand corner of the test vessel. The condensing plate thickness and the vessel thickness are both 30.48 cm. Each condensing plate was divided into six sections, so that the temperature of condensing plate was kept at a fixed value by cooling each section individually. Coolant water passed through the cooling plates. The other boundary walls were adiabatic conditions. A mixture of air and steam entered the facility from nineteen inlets along the bottom of the test section. The total system pressure remained constant at 1 bar, and the aluminum condensing plates were held at a temperature of approximately 30°C. This paper simulates four experiments with different air mass fractions, as shown in Table 1.

Since the mixed gas temperature differences and concentration differences in the vessel thickness direction are small (the side walls are adiabatic), the heat and mass transfer in the vessel can be simplified to two-dimensional simulation. Steam is injected into the bottom of the test vessel through 19 evenly spaced nozzles, and the 19 nozzles were simplified to one inlet in the simulation. The geometry was meshed with structural grids using Gambit 2.4.6; the near wall elements were refined to insure that y+ was less than 1. The geometry and mesh of the scaled AP600 containment are shown in Figure 3. The system operating pressure was 1 bar. The constant wall temperature boundary condition was used at the top condensation wall and the vertical condensation wall, the other walls were adiabatic. No-slip boundary condition was used for all the walls. The inlet superheated steam pressure was 1.7 bars and the inlet steam temperature was 125.13°C; the steam mass flow rate was adjusted to reach the test steady state.

2.1.2. AP1000 Containment. Since this paper mainly focuses on the influences of noncondensable gases on convective condensation, the pressure vessel and other equipment in the AP1000 containment were ignored in this simulation. Due to the large free spaces in the reactor containment, this assumption will not influence the overall natural convection flow pattern. As shown in Figure 4, the upper head is 11.4681 m high, and the total height is 54.1655 m [24]. Since the geometry is axisymmetric, the two-dimensional axisymmetric model is used. After the LOCA accident, the AP1000 reactor core will be flooded; water is heated and evaporates from the containment bottom. So the containment bottom was set as an evaporation wall, which supplies saturation steam continuously. The simplified AP1000 containment geometry is shown in Figure 4(a). The geometry was meshed using Gambit 2.4.6; the near wall elements were refined to insure that y+ was less than 1. The mesh of AP1000 containment is shown in Figure 4(b).

2.2. Condensation Model and Boundary Conditions. The condensation model in this paper includes the continuity, momentum, and energy conservation equations along with the species conservation equation. The standard k-ε model was used in this work for the closure of the Reynolds stress term. The enhanced wall treatment was used for the near wall treatment. The Reynolds Averaged Navier Stockes equations and the transport equations for k and ε can be found in [23, 25]. Gravity is the driven force of natural convection. The mixture gas gravity was considered in the simulation.

The condensation process was modeled by introducing appropriate source terms into the mass, momentum, energy, and species conservation equations in cells most adjacent to the wall. The source terms were incorporated into the FLUENT code through User Defined Functions (UDFs). The condensation film was not modeled.

The detailed expressions of the source terms of the governing equations have been presented by Fu et. al [23]. However, they are described here with more explanation. According to Fick's first law of diffusion and the solution of Stefan flow, the steam condensation mass flux in the cells most adjacent to the condensation wall can be expressed as [10]

$$m''_{cond} = \frac{D_{vn} M_v P_{total}}{RT} \frac{\ln X_{n,c} - \ln X_{n,w}}{\Delta r} \quad (2)$$

where Δr is the thickness of cell most adjacent to the condensation wall, $X_{n,c}$ is the molar fraction of noncondensable gases in the cell most adjacent to the condensation wall,

Table 1: Conditions of the simulated AP600 containment atmospheric experiments.

Test	Bulk pressure (bar)	Air mass fraction	Bulk temperature (°C)	Wall temperature (°C)
202	1.0	0.8618	60.65	28.60
203	1.0	0.7900	69.23	29.40
213	1.0	0.6472	79.68	34.00
219	1.0	0.4159	89.72	30.30

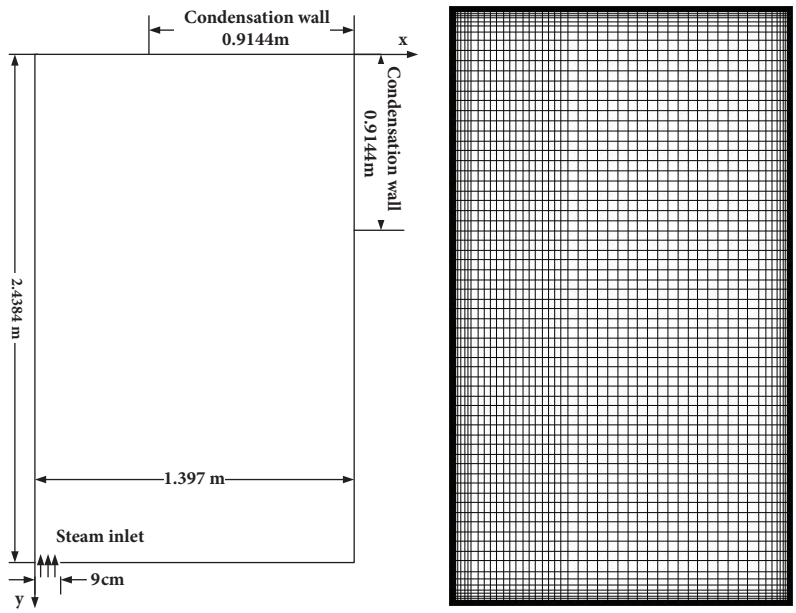

(a) Geometry (b) Mesh

Figure 3: Geometry and mesh of Anderson's scaled AP600 containment experiments. (a) Geometry. (b) Mesh.

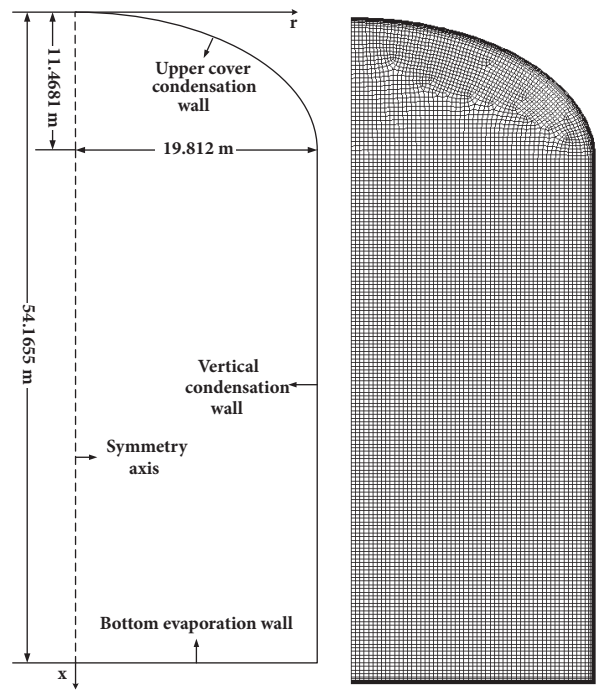

(a) Geometry (b) Mesh

Figure 4: Geometry and mesh of AP1000 containment. (a) Geometry. (b) Mesh.

$X_{n,w}$ is the molar fraction of noncondensable gases at the condensation wall, calculated by $X_{n,w} = (1 - P_{v,w})/P_{total}$, $P_{v,w} = P_{sat}(T_w)$ is the saturation pressure based on the wall temperature, D_{vn} is the laminar mass diffusion coefficient, and R is the gas constant.

Since the interface is impermeable to air, the gas mixture mass source term is equivalent to the steam source term:

$$S_v = S_{mass} = m''_{cond} \frac{A_{cell,wall}}{V_{cell}} \tag{3}$$

The momentum source term can be expressed as

$$S_{x-mom} = u_x m''_{cond} \frac{A_{cell,wall}}{V_{cell}} \tag{4}$$

$$S_{r-mom} = u_r m''_{cond} \frac{A_{cell,wall}}{V_{cell}} \tag{5}$$

The energy source term is

$$S_{energy} = m''_{cond} \frac{A_{cell,wall}}{V_{cell}} h_v \tag{6}$$

If the steam molar fraction in the cell is larger than the steam molar fraction at the condensation wall, $X_{v,c} > X_{v,w}$, condensation takes place and the source terms are calculated according to (3)-(6). Otherwise, the source terms are zero. If the steam molar fraction in the cell is smaller than the steam molar fraction at the bottom evaporation wall, $X_{v,c} < X_{v,w}$, evaporation takes place. The source terms of evaporation are similar to the condensation source terms, and the evaporation source terms are positive, while the condensation source terms are negative.

The constant wall temperature boundary was set at the containment upper header condensation wall and the vertical condensation wall. The bottom evaporation wall was also set as constant wall temperature, and the steam mass fraction was 1. The mixture gas was considered as ideal gas, with the mixture gas density calculated based on the ideal gas state equation. The specific heat, thermal conductivity, viscosity, and other properties of each species were set as a polynomial variation of temperature. The properties of the mixture gas were calculated by the mass-weighted average properties of each species. The governing equations were discretized using the finite volume method. The convection terms of the equations were discretized using the Quick scheme. SIMPLE method was used for the pressure-velocity coupling. Convergence determination of the calculations was based on the history of several variables chosen at different locations of the computational domain as well as the classical residual decrement.

3. Natural Convective Condensation with Noncondensable Gases in Scaled AP600 Containment Experiments

3.1. Numerical Method Verification. In order to verify the numerical model and the ability of the developed method to simulate natural convective condensation with noncondensable gases, Anderson's AP600 containment experiment was first simulated. The heat transfer coefficients from the simulation results and Anderson's test data are shown in Figure 5. It can be seen that the heat transfer coefficient decreases with the increasing of air mass fraction, and the deviations between the simulation results and the test data are within 5%. The CFD simulation method in this work can be used to simulate the natural convective condensation process with the presence of noncondensable gases.

3.2. Velocity, Species, and Density Distributions. Figure 6 shows the velocity and streamlines in the scaled containment vessel. It clearly shows that natural convection is established in the vessel. The gas mixture flows upward at the left and then hits the top wall and flows downward along the right wall. Then the noncondensed gas mixture (air and steam) flows to the left, after mixing with the newly added steam from the nozzle, and the mixtures flow upward again. The maximum velocity of 0.95 m/s is obtained at the right condensation wall. The gas mixture releases heat and steam condensates at the top and right walls, leading to the decrease of temperature and stream mass fraction.

Figure 7 shows the steam mass fraction distribution in the vessel. It is shown that steam mass fraction decreases significantly near the condensation walls. There exists a thin layer with low steam mass fraction near the condensation walls. The volume averaged steam mass fraction is about 0.3, while in the near wall region the steam mass fraction can reach 0.1 or even lower. The minimum steam mass fraction is in the right upper corner of the vessel.

Figure 8 shows the density distribution in the scaled containment vessel. It can be seen that the densities near the top and right vertical wall are much larger than the average density and that near the left wall. This is mainly due to the larger air mass fraction of gas mixture in these regions. The molecular weight of air is about 29 g/mol, while that of steam is only 18 g/mol. The density decrements induced by temperatures in these regions are much smaller compared with mass fraction. This is the key difference between natural convection of condensation with noncondensable gases and the conventional natural convection. So the driving force of natural condensation with noncondensable gases is mainly the mass fraction difference but not the temperature difference. From this finding, we can deduce that the molecular weight of the noncondensable gases will also influence the natural convection and the total heat transfer coefficient.

3.3. Heat and Mass Transfer. The distributions of condensation mass flux along the top wall with various air mass fractions are shown in Figure 9. It can be seen that the condensation mass flux decreases with the increasing of air

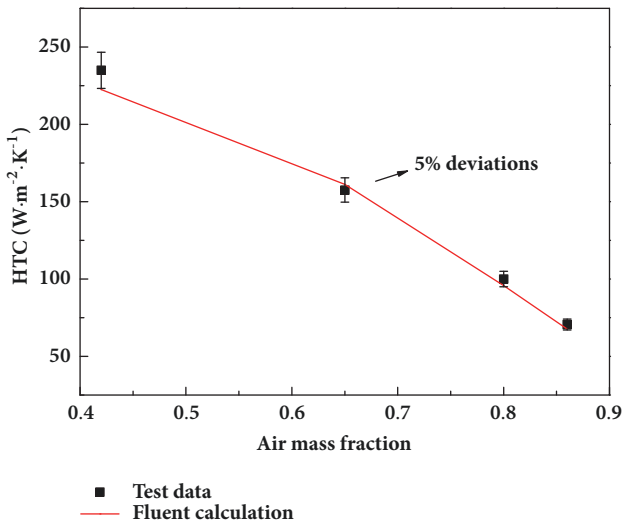

Figure 5: Comparison of simulation results with the scaled AP600 containment test data.

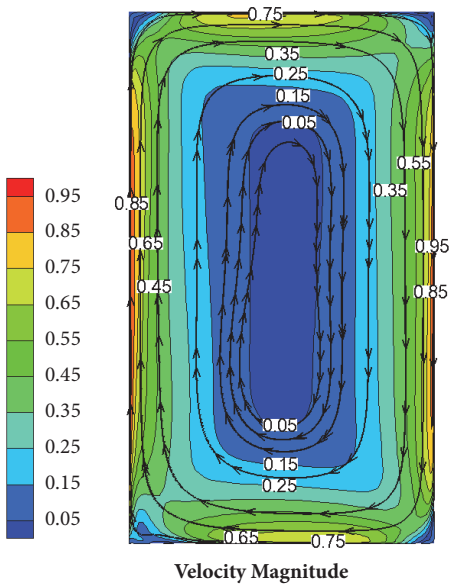

Figure 6: Gas mixture velocity contour and streamlines in the scaled AP600 containment.

mass fraction. The condensation mass flux also decreases along the flow direction. This is because the concentration difference between the bulk and the wall decreases gradually in the flow direction. The distributions of condensation mass flux along the vertical condensation wall with various air mass fractions are shown in Figure 10. Figure 10 also shows that the condensation mass flux decreases with the increasing of air mass fraction. The condensation mass flux also decreases along the flow direction. The comparison of Figures 9 and 10 shows that the condensation mass flux at the top condensation wall is obviously larger than that at the vertical condensation wall.

The comparison of total heat flux at the top wall and the right vertical wall with various air mass fractions is shown in Figure 11. The heat flux at the top wall is larger than that at the right vertical wall, especially for the low air mass fraction condition. This is due to the larger mass fraction of steam at the top wall as shown in Figure 7.

4. Natural Convective Condensation with Noncondensable Gases in AP1000 Containment

After a large LOCA (loss of coolant accident) accident, steam will be released in the containment fill with atmospheric pressure of air. With the progress of the accident, the bottom of the containment will be flooded, and the residual heat will heat the water at the bottom of the containment. Steam evaporates from the bottom and condensates on the inner surface of the containment. For a typical condition after a large LOCA accident, the temperature in the containment is 380.35 K, the gas mixture pressure is 0.2565MPa [26], the steam molar fraction is 50%, and the steam mass fraction is 39%. The outer wall temperature of containment is 100°C. These conditions will be used for the simulation.

4.1. Velocity, Species, Temperature, and Density Distributions. The operation pressure is 0.2565 MPa, the condensation wall temperature is set as 373.15 K, and the temperature of gas mixture is 380.35 K. The velocity contour and streamlines are shown in Figure 12. It can be seen that gas mixture flows upward along the symmetry axis and then hits the upper head and flows downward along the vertical wall, until it reaches the bottom evaporation wall. The maximum velocity of 2.95 m/s is reached at the central axis of the containment. The velocity near the upper header and right vertical wall can be more than 1 m/s.

The distribution of gas mixture temperature is shown in Figure 13. It can be seen that the gas mixture near the condensation wall has low temperature, and the gas mixture near the evaporation wall has high temperature. However, the maximum temperature difference in the reactor containment is only 21°C.

The distribution of steam mass fraction is shown in Figure 14. The steam mass fraction increases after flowing over the bottom evaporation wall and reaches the maximum. Then the steam mass fraction decreases when approaching the condensation wall.

Figure 15 shows gas mixture density contour in the reactor containment. The gas mixture density near the condensation wall is the largest, and the value is about 2.1 kg/m^3. The gas mixture density near the evaporation wall is the smallest, and the value is about 1.8 kg/m^3. The difference is about 16.7%. This density difference is the origin of the driving force. Using the ideal gas model, the 21°C temperature difference shown in Figure 13 can only introduce about 5% density difference. So the other 10% density difference is caused by the mass fraction difference shown in Figure 14. This also supports the conclusion that was reached in the simulation of scaled AP600 containment experiments.

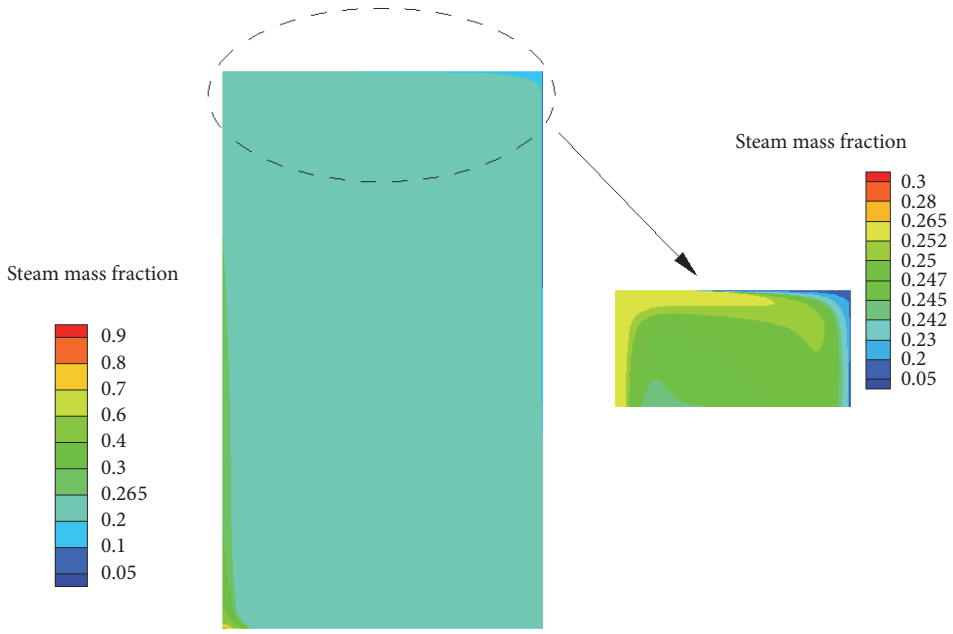

Figure 7: Steam mass fraction in the scaled AP600 containment.

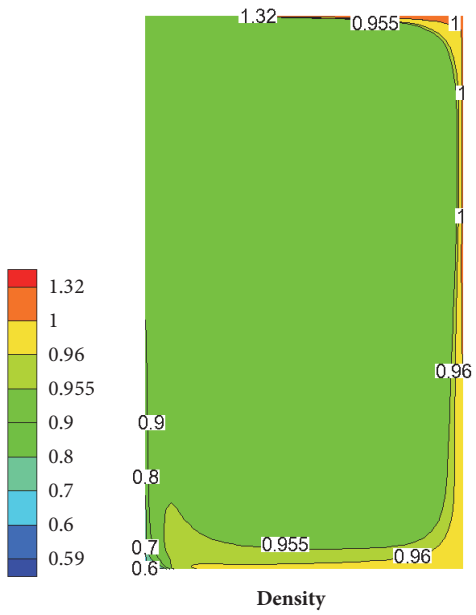

Figure 8: Gas mixture density in the scaled AP600 containment.

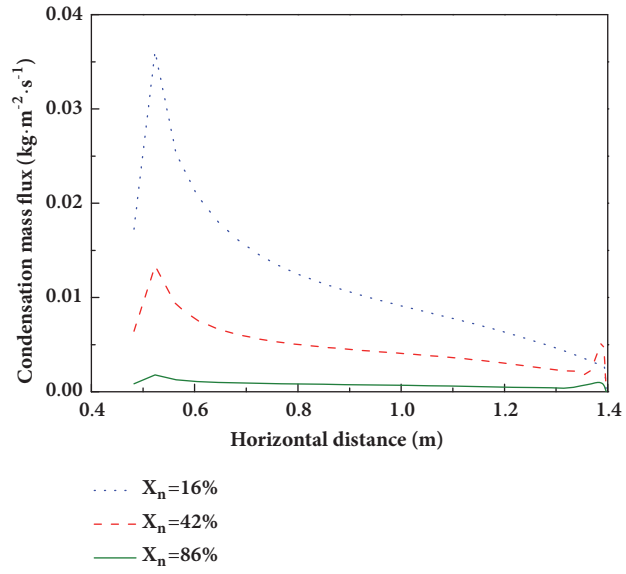

Figure 9: The distribution of condensation mass flux along the top wall.

4.2. Heat and Mass Transfer. The distributions of condensation mass flux and heat flux along the upper header and vertical walls are shown in Figure 16. The horizontal axis represents the distance along the wall from the axis. The dotted line represents the separation point for the upper head and the vertical wall. It can be seen that the condensation mass flux and heat flux at the upper cover (or upper head) wall are larger than that at the vertical wall. This is because the gas mixture flows upward and hits the upper head at x=0 m, which will make the heat and mass transfer coefficients larger. Another reason is that the steam mass fraction here is the highest, so the condensation mass flux will be the highest. With the condensation of steam, the concentration of steam decreases along the flow direction, leading to the decrease of the condensation mass flux and heat flux. It can also be obtained from the Fluent calculation that the heat transfer rate at the containment upper cover is about 35.1% of the

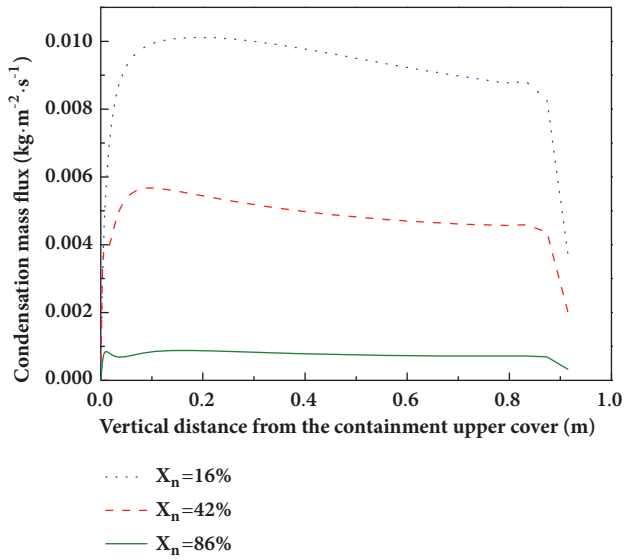

FIGURE 10: The distribution of condensation mass flux along the vertical condensation wall.

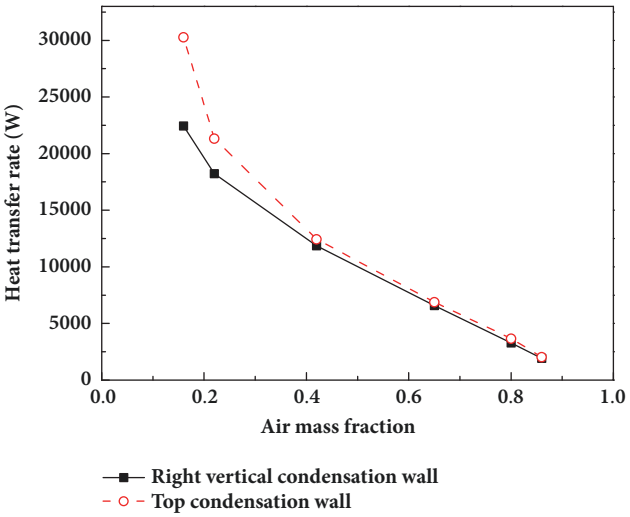

FIGURE 11: Comparison of heat transfer rate at right wall and top wall.

total heat transfer rate, even though the upper cover area is only 25.4% of the total condensation area. We can get a conclusion that the condensation heat transfer at the upper cover is essential for the containment cooling system.

The influence of temperature difference on heat flux was investigated by varying the temperature difference between the evaporation wall and the condensation wall. With the increasing of the temperature difference between the evaporation wall and the condensation wall, the driving force increases, resulting in the increasing of the heat flux, as shown in Figure 17. It can also be seen that the total heat transfer of gas mixture mainly depends on the condensation heat transfer, while the contribution of convective heat transfer of gas mixture is little.

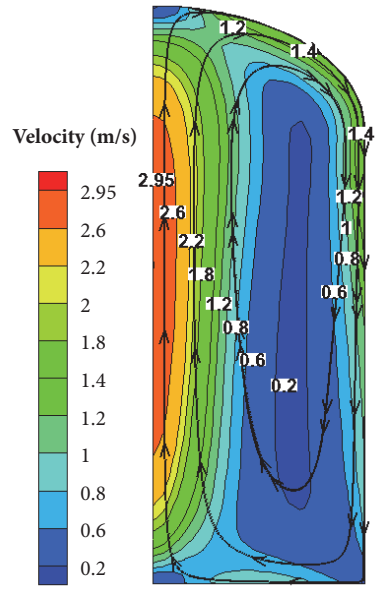

FIGURE 12: Velocity contour and streamlines in the AP1000 containment.

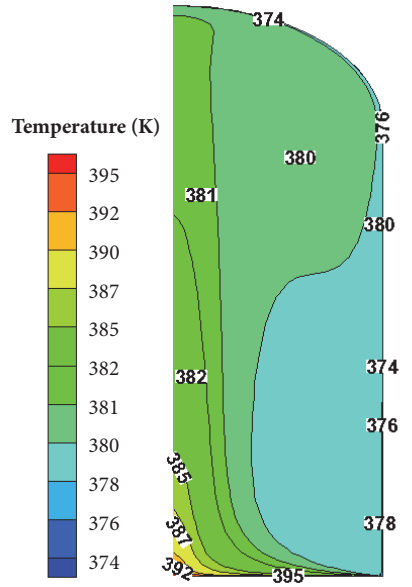

FIGURE 13: Temperature contour in the AP1000 containment.

4.3. Effects of Hydrogen in the Noncondensable Mixture. The effects of small molecular weight gas (such as hydrogen) on natural convective condensation with noncondensable gases mainly consist of two aspects. On one hand, the hydrogen will increase the diffusion coefficient, which means steam diffuses more easily from the small molecular weight gas compared to the large molecular weight gas. On the other hand, hydrogen will decrease the density of gas mixture when steam condenses, leading to the decrease of the natural circulation driven force. So, hydrogen affects the natural convective condensation with noncondensable processes by increasing

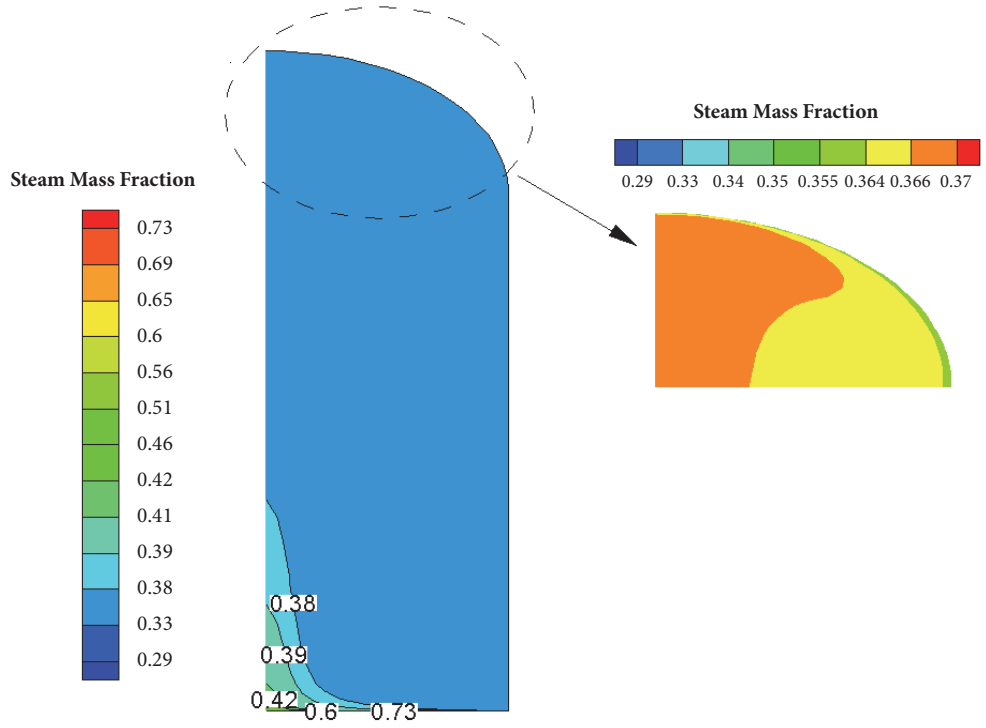

Figure 14: Steam mass fraction contour in the AP1000 containment.

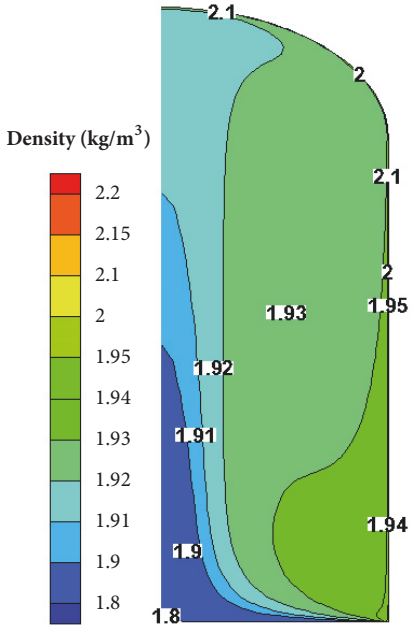

Figure 15: Density contour in the AP1000 containment.

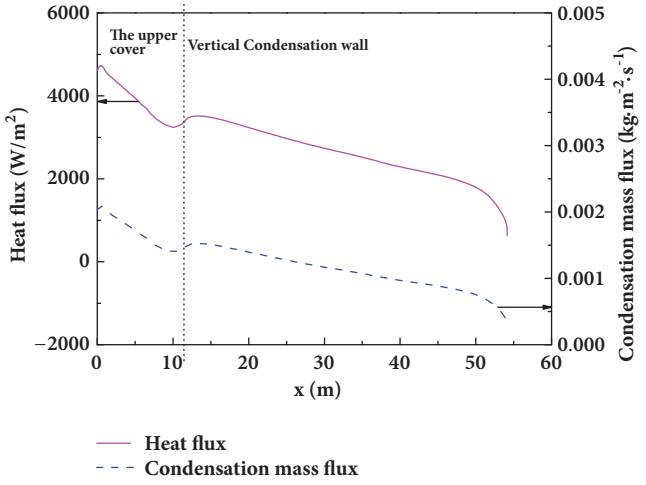

Figure 16: The distributions of heat flux and condensation mass flux.

the steam diffusion and decreasing the buoyancy force. For natural convection, buoyancy force is very important.

The operation pressure is 0.2565 MPa, the temperature of bottom evaporation wall is set as 395 K, the temperature of condensation wall is set as 373.15 K, and the steam mole fraction of total gas mixture is 50%, which is the same as previously done. Cases with different percentage of hydrogen are simulated. The percentage of hydrogen in the noncondensable gases changes from 0% to 100%. With the increase of the hydrogen mole fraction, the steam diffusion coefficient will increase, as shown in Figure 18. Figure 19 shows the maximum concentration (or species) gradient and maximum gas mixture velocity in the containment will decrease with increasing hydrogen concentration. The effect of hydrogen

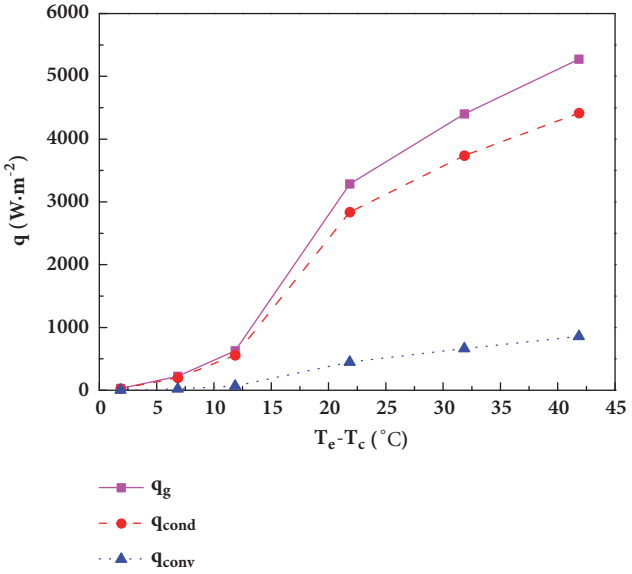

Figure 17: Effect of temperature difference on heat flux.

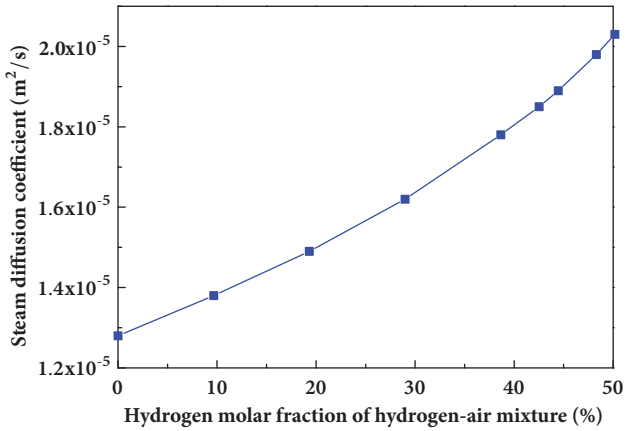

Figure 18: Steam diffusion coefficient with different hydrogen molar fractions.

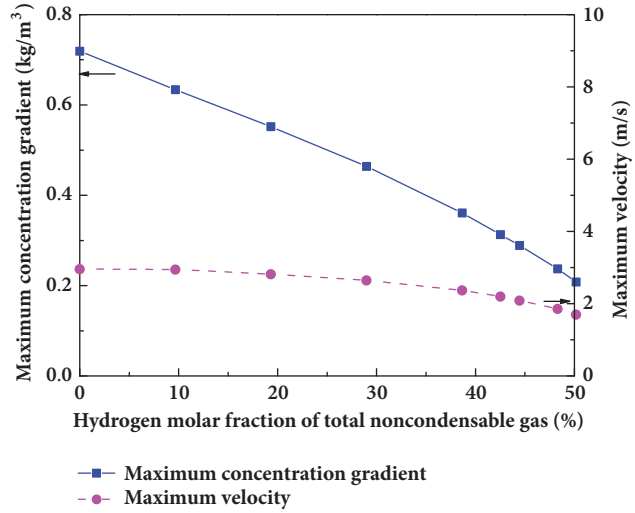

Figure 19: Maximum concentration gradient and velocity with different hydrogen molar fractions.

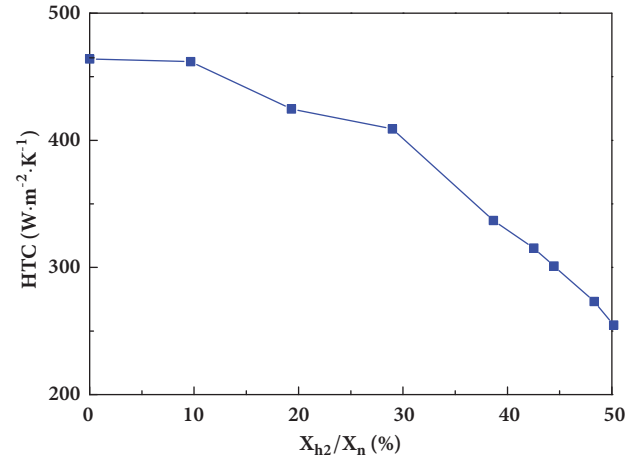

Figure 20: Heat transfer coefficient with different hydrogen molar fractions.

on heat transfer coefficient of gas mixture is shown in Figure 20. The heat transfer coefficient decreases with the increase of hydrogen mole fraction. When the hydrogen mole fraction of total noncondensable gases is larger than 30%, the heat transfer coefficient will decrease sharply. When the hydrogen molar concentration of total noncondensable gases reaches 50%, the heat transfer coefficient of steam-hydrogen-air mixture is only about 55% of the steam-air mixture.

5. Conclusions

Simulation of natural convective steam condensation with noncondensable gases in reactor containment was realized by adding source terms in commercial software. The calculation results were compared to the scaled AP600 containment atmospheric experiments. Then the natural convective steam condensation with noncondensable gases in the AP1000 reactor containment was simulated. The detailed velocity, temperature, mass fraction, and density fields and their influences on the heat and mass fluxes were analyzed. The influences of hydrogen on the natural convection and heat and mass flux were also investigated. The conclusions are as follows.

(1) The simulation results of the total heat transfer coefficients compared well with the scaled AP600 containment test data. The deviations are within 5% for different mass fraction of air. The method can be used to simulate natural convective condensation with the presence of noncondensable gases.

(2) The key difference between natural convection of steam condensation with noncondensable gases and the conventional natural convection is the origin of the density difference or the driving force. The mass fraction difference caused density difference which will influence the driving force of natural convection

of steam condensation with noncondensable gases. It is related to the mole fraction of noncondensable gases and also the molecular weight of the steam and noncondensable gases.

(3) The temperature, steam mass fraction, density, and velocity contours for the natural convective condensation processes in AP600 scaled containment experiments and AP1000 containment were obtained. The total heat transfer of gas mixture mainly depends on the condensation heat transfer, while the contribution of convective heat transfer of gas mixture is little. The condensation mass flux decreases with the increase of air mass fraction. The condensation heat transfer at the upper cover is essential for the containment cooling.

(4) Hydrogen affects the natural convective condensation processes by increasing the steam diffusion and decreasing the buoyance force. Hydrogen will decrease natural convective condensation heat transfer coefficient by 45% when it contributes to 50% of the molar fraction of the noncondensable gases.

Nomenclature

A: Surface area (m^2)
D_{vn}: Mass diffusion coefficient (m^2/s)
h: Heat transfer coefficient ($W \cdot m^{-2} \cdot K^{-1}$) or enthalpy (J/kg)
h_v: Enthalpy of steam (J/kg)
M: Molecular weight (kg/mol)
m''_{cond}: Condensation mass flux ($kg \cdot m^{-2} \cdot s^{-1}$)
Nu: Nusselt number
P: Pressure (Pa)
q: Heat flux ($W \cdot m^{-2}$)
R: Gas constant
Re: Reynolds number
S_{energy}: Source term for energy ($W \cdot m^{-3} \cdot s^{-1}$)
S_{mass}: Source term for mass ($kg \cdot m^{-3} \cdot s^{-1}$)
S_v: Source term for steam species ($kg \cdot m^{-3} \cdot s^{-1}$)
S_{x-mom}: Source term of axial momentum ($N \cdot m^{-3} \cdot s^{-1}$)
S_{r-mom}: Source term of radial momentum ($N \cdot m^{-3} \cdot s^{-1}$)
T: Temperature (K)
u: Velocity (m/s)
V: Volume (m^3)
X: Molar fraction.

Subscripts

b: Bulk
cond: Condensation
conv: Convective
g: Gas mixture
i: Interface
l: Condensation film
n: Noncondensable gas
v: Steam
w: Condensation wall.

Data Availability

The data used to support the findings of this study are included within the article.

Conflicts of Interest

The authors declare that there are no conflicts of interest regarding the publication of this paper.

Acknowledgments

This work was financially supported by the National Natural Science Foundation of China (51576103) and the National S&T Major Project (Grant No. ZX06901).

References

[1] W. Fu, X. W. Li, and X. X. Wu, "Natural convective condensation with non-condensable gases in the reactor containment and its enhancement," in *Proceedings of the Asian Conference on Thermal Sciences 2017 (1st ACTS)*, Jeju Island, Korea, 2017.

[2] D. F. Othmer, "The condensation of steam," *Industrial and Engineering Chemistry*, vol. 21, no. 6, pp. 576–583, 1929.

[3] M. L. Corradini, "Turbulent condensation on a cold wall in the presence of a noncondensable gas," *Nuclear Technology*, vol. 64, no. 2, pp. 186–195, 1984.

[4] Y. Li, H. Zhang, J. Xiao, J. R. Travis, and T. Jordan, "Numerical investigation of natural convection inside the containment with recovering passive containment cooling system using GASFLOW-MPI," *Annals of Nuclear Energy*, vol. 114, pp. 1–10, 2018.

[5] H. Uchida, A. Oyama, and Y. Togo, *Evaluation of post-incident cooling systems of light water power reactors*, Tokyo University, Tokyo, Japan, 1964.

[6] A. A. Dehbi, *The effects of noncondensable gases on steam condensation under turbulent natural convection conditions*, Massachusetts Institute of Technology, 1991.

[7] S. Z. Kuhn, *Investigation of heat transfer from condensing steam-gas mixtures and turbulent films flowing downward inside a vertical tube*, University of California, Berkeley, USA, 1995.

[8] M. H. Anderson, *Steam condensation on cold walls of advanced PWR containments*, University of Wisconsin-Madison, USA, 1998.

[9] J. Malet, E. Porcheron, and J. Vendel, "OECD International Standard Problem ISP-47 on containment thermal-hydraulics - Conclusions of the TOSQAN part," *Nuclear Engineering and Design*, vol. 240, no. 10, pp. 3209–3220, 2010.

[10] F. Kreith, R. Manglik, and M. Bohn, *Principles of Heat Transfer*, Harper and Row, New York, NY, USA, 2010.

[11] P. F. Peterson, V. E. Schrock, and T. Kageyama, "Diffusion layer theory for turbulent wapor condensation with noncondensable gases," *Journal of Heat Transfer*, vol. 115, no. 4, pp. 998–1003, 1993.

[12] S. Zhang, X. Cheng, and F. Shen, "Condensation heat transfer with non-condensable gas on a vertical tube," *Energy and Power Engineering*, vol. 10, no. 04, pp. 25–34, 2018.

[13] L. E. Herranz, M. H. Anderson, and M. L. Corradini, "A diffusion layer model for steam condensation within the AP600 containment," *Nuclear Engineering and Design*, vol. 183, no. 1-2, pp. 133–150, 1998.

[14] M. H. Kim and M. L. Corradini, "Modeling of condensation heat transfer in a reactor containment," *Nuclear Engineering and Design*, vol. 118, no. 2, pp. 193–212, 1990.

[15] H. Zhang, Y. Li, J. Xiao, and T. Jordan, "Uncertainty analysis of condensation heat transfer benchmark using CFD code GASFLOW-MPI," *Nuclear Engineering and Design*, vol. 340, pp. 308–317, 2018.

[16] X. W. Li, X. X. Wu, and S. Y. He, "Numerical simulation of the heat and mass transfer process of convective condensation with non-condensable gas," *Journal of Engineering Thermophysics*, vol. 34, no. 2, pp. 302–306, 2013 (Chinese).

[17] A. Dehbi, F. Janasz, and B. Bell, "Prediction of steam condensation in the presence of noncondensable gases using a CFD-based approach," *Nuclear Engineering and Design*, vol. 258, pp. 199–210, 2013.

[18] J. Su, Z. Sun, and D. Zhang, "Numerical analysis of steam condensation over a vertical surface in presence of air," *Annals of Nuclear Energy*, vol. 72, pp. 268–276, 2014.

[19] T.-H. Phan, S.-S. Won, and W.-G. Park, "Numerical simulation of air–steam mixture condensation flows in a vertical tube," *International Journal of Heat and Mass Transfer*, vol. 127, pp. 568–578, 2018.

[20] M. Punetha and S. Khandekar, "A CFD based modelling approach for predicting steam condensation in the presence of non-condensable gases," *Nuclear Engineering and Design*, vol. 324, pp. 280–296, 2017.

[21] H. Bian, Z. Sun, M. Ding, and N. Zhang, "Local phenomena analysis of steam condensation in the presence of air," *Progress in Nuclear Energy*, vol. 101, pp. 188–198, 2017.

[22] H. Bian, Z. Sun, N. Zhang, Z. Meng, and M. Ding, "A preliminary assessment on a two-phase steam condensation model in nuclear containment applications," *Annals of Nuclear Energy*, vol. 121, pp. 615–625, 2018.

[23] W. Fu, X. Li, and X. Wu, "Numerical investigation of convective condensation with the presence of non-condensable gases in a vertical tube," *Nuclear Engineering and Design*, vol. 297, pp. 197–207, 2016.

[24] *The AP1000 European DCD. UK AP1000 Safety, Security, and Environmental Report*, 2007.

[25] *ANSYS Fluent 15.0 Theory Guide*, ANSYS Inc, 2013.

[26] F. C. Rahim, M. Rahgoshay, and S. K. Mousavian, "A study of large break LOCA in the AP1000 reactor containment," *Progress in Nuclear Energy*, vol. 54, no. 1, pp. 132–137, 2012.